Analysis of Finite Grid Structures with Lenses in Quasi-Optical Systems

Todd W. Nuteson, *Member, IEEE,* Huan-Sheng Hwang, *Student Member, IEEE,* Michael B. Steer, *Senior Member, IEEE,* Krishna Naishadham, *Member, IEEE,* James Harvey, *Member, IEEE,* and James W. Mink, *Fellow, IEEE*

***Abstract*—A full-wave moment-method technique developed for the analysis of quasi-optical (QO) systems is used to model finite grid structures in a lens system. This technique incorporates an electric-field dyadic Green's function for a grid centered between two lenses. This is derived by separately considering paraxial and nonparaxial fields. Results for the driving point reflection coefficient of a 3 × 3 and 5 × 5 grid in the lens system are computed and compared with measurements.**

***Index Terms*—Green's function, moment methods.**

I. Introduction

QUASI-OPTICAL (QO) techniques provide a means for combining power from numerous solid-state millimeter-wave sources without the use of lossy metallic interconnections. Power from the sources in an array is combined over a distance of many wavelengths to channel power predominantly into a single paraxial mode, see Fig. 1. Progress toward large, high-powered, efficient arrays is hampered by the relatively crude state of design technology including the lack of suitable computer-aided engineering (CAE) tools. In particular, the many unit active circuits in a large array cannot be individually optimized for efficiency and stability. This is because no process has been developed to model impedances and simulate the dynamic behavior of a finite array where most of the array elements see different circuit conditions.

The QO modeling approach pioneered by the authors [1]–[5], uses a full-wave moment-method technique and an electric-field QO dyadic Green's function. A series of developments [1]–[3] culminated in a straightforward methodology for developing a novel Green's function of a QO system. The electric-field dyadic Green's function of a QO system is derived in two parts: one part describing the effect of the QO paraxial fields and the other part describing the remaining fields. This form of the dyadic Green's function is particularly convenient for QO systems because of its relative ease of development. It did, however, necessitate the development of an advanced method of moments (MoM) approach combining spatial-domain and spectral-domain techniques to model a QO open-cavity resonator [4]. With this formulation, the field solver can be conveniently used in the development of circuit-level models of QO systems.

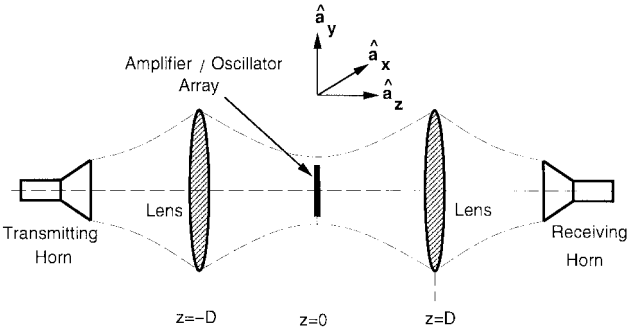

Fig. 1. QO lens system configuration with a centered amplifier array.

In this paper, the authors present the derivation of the electric-field dyadic Green's function for the lens system shown in Fig. 1 and incorporate it into the moment-method routine developed in [4]. Simulations and measurements of a unit cell, a 3 × 3 grid, and a 5 × 5 grid, all on dielectric substrates and placed in the lens system, are performed to verify the Green's function. Results for finite grid structures in free space were presented in [5].

II. Dyadic Green's Function of Lens System

The approach used in [2], [3] to develop a dyadic Green's function for a QO open-cavity resonator is used here to develop a Green's function for the system shown in Fig. 1. As usual, the electric field

$$\mathbf{E}(\mathbf{r}) = \int_{\Omega'} \overline{\overline{\mathbf{G}}}_E(\mathbf{r}|\mathbf{r}') \cdot \mathbf{J}_S(\mathbf{r}')\, dv' \tag{1}$$

where $\overline{\overline{\mathbf{G}}}_E$ is the electric-field dyadic Green's function and $\mathbf{J}_S$ is the electric-current density source used to excite the fields, the primed notation $r' = \{x', y', z'\}$ denotes the source coordinates and the unprimed notation $r = \{x, y, z\}$ denotes the observation coordinates. The special insight in

Manuscript received October 17, 1996; revised January 24, 1997. This work was supported in part by the U.S. Army Research Office under Grant DAAH04-95-1-0536 and by a subcontract from Scientific Research Associated, Inc. under U.S. Army Missile Command Contract DAAH01-95-C-R111.

T. W. Nuteson, H. S. Hwang, M. B. Steer, and J. W. Mink are with the Electronics Research Laboratory, Department of Electrical and Computer Engineering, North Carolina State University, Raleigh, NC 27695-7911 USA.

K. Naishadham is with the Department of Electrical Engineering, Wright State University, Dayton, OH 45435 USA.

J. Harvey is with the U.S. Army Research Office, Research Triangle Park, NC 27709-2211 USA.

Publisher Item Identifier S 0018-9480(97)02909-8.

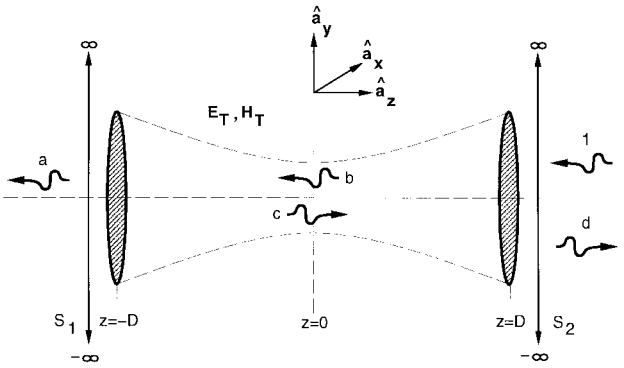

Fig. 2. Cross section of the lens system showing the test field.

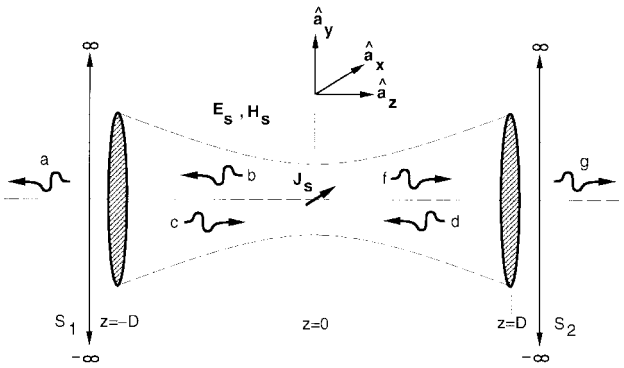

Fig. 3. Cross section of the lens system showing the source field.

the technique discussed here is the derivation of $\overline{\overline{\mathbf{G}}}_E$ in the following two parts:

$$\overline{\overline{\mathbf{G}}}_E = \overline{\overline{\mathbf{G}}}_{En} + \overline{\overline{\mathbf{G}}}_{Em} \tag{2}$$

where $\overline{\overline{\mathbf{G}}}_{En}$ and $\overline{\overline{\mathbf{G}}}_{Em}$ refer to the nonmodal and modal fields, respectively. Thus, the paraxial fields (QO modes), which are largely responsible for distant interactions in the QO system and the corrected free-space (nonmodal) interactions responsible for near neighbor interactions, are separately considered. The derivation of these parts is described below.

A. Modal Component—$\overline{\overline{\mathbf{G}}}_{Em}$

In the lens system, the modal electric fields are approximated as the superposition of Hermite–Gaussian traveling wavebeams, $E^{\pm}_{mn}$ (given in [1], [4]). The first step in deriving the modal component ($\overline{\overline{\mathbf{G}}}_{Em}$) of the Green's function is to introduce a test field in the system which is excited by a single wave-beam mode with unit amplitude at $z \gg D$ as shown in Fig. 2. The test field

$$\mathbf{E}_{T,\,st} = \begin{cases} a_{st}E^{-}_{st}\,\hat{\mathbf{a}}_x, & z < -D \\ (c_{st}E^{+}_{st} + b_{st}E^{-}_{st})\,\hat{\mathbf{a}}_x, & -D < z < D \\ (d_{st}E^{+}_{st} + E^{-}_{st})\,\hat{\mathbf{a}}_x, & z > D \end{cases} \tag{3}$$

where the coefficients are determined by the boundary conditions at each lens in terms of transmission and reflection coefficients. At the first lens ($z = -D$) the transmission and reflection coefficients are $T_{1,\,st}$ and $R_{1,\,st}$, respectively. $T_{2,\,st}$ and $R_{2,\,st}$ are the corresponding coefficients for the second lens at $z = D$.

The next step in the derivation is to introduce a source. The source field excited by a current density source $\mathbf{J}_S = J_x\hat{\mathbf{a}}_x$, as shown in Fig. 3, is

$$\mathbf{E}_S = \sum_{mn} \begin{cases} a_{mn}E^{-}_{mn}\,\hat{\mathbf{a}}_x, & z < -D \\ (c_{mn}E^{+}_{mn} + b_{mn}E^{-}_{mn})\,\hat{\mathbf{a}}_x, & -D < z < 0 \\ (f_{mn}E^{+}_{mn} + d_{mn}E^{-}_{mn})\,\hat{\mathbf{a}}_x, & 0 < z < D \\ g_{mn}E^{+}_{mn}\,\hat{\mathbf{a}}_x, & z > D \end{cases} \tag{4}$$

being the superposition of all QO modes. The coefficients in (4) are determined using the same transmission and reflection coefficients used in the test-field solution. For the source field, there are five equations and six unknowns so the solution is found in terms of g_{mn}, which in turn, is found using the Lorentz reciprocity theorem. For this problem, the Lorentz reciprocity theorem is stated as follows:

$$\oint_S (\mathbf{E}_T \times \mathbf{H}_S - \mathbf{E}_S \times \mathbf{H}_T)\cdot\hat{\mathbf{n}}\,ds = -\int_\Omega \mathbf{E}_T \cdot \mathbf{J}_S\,dv \tag{5}$$

where the surface $S = S_1 + S_2$ bounds the volume Ω. The magnetic source and test fields, $\mathbf{H}_S$ and $\mathbf{H}_T$, are determined by making a TEM approximation which is valid near $z = 0$, since the phase fronts are flat here. Thus

$$g_{mn} = \frac{-T_{2,mn}}{2(1 - R_{1,\,mn}\psi_{1,\,mn}R_{2,\,mn}\psi_{2,\,mn})} \cdot \int_\Omega (R_{1,\,mn}\psi_{1,\,mn}E^{+}_{mn} + E^{-}_{mn})\,J_x\,dv. \tag{6}$$

A similar result is obtained for a y-directed current source. Combining (1) and (4), the modal Green's function is as shown in (7) at the bottom of the page, where $\overline{\overline{\mathbf{I}}}_T$ is the transverse

$$\overline{\overline{\mathbf{G}}}_{Em} = -\sum_{mn} \frac{\acute{E}_{mn}}{2(1 - R_{1,\,mn}\psi_{1,\,mn}R_{2,\,mn}\psi_{2,\,mn})}\,\overline{\overline{\mathbf{I}}}_T \begin{cases} T_{1,\,mn}(1 + R_{2,\,mn}\psi_{2,\,mn})E^{-}_{mn}, & z < -D \\ (1 + R_{2,\,mn}\psi_{2,\,mn})(R_{1,\,mn}\psi_{1,\,mn}E^{+}_{mn} + E^{-}_{mn}), & -D < z < 0 \\ (1 + R_{1,\,mn}\psi_{1,\,mn})(E^{+}_{mn} + R_{2,\,mn}\psi_{2,\,mn}E^{-}_{mn}), & 0 < z < D \\ T_{2,\,mn}(1 + R_{1,\,mn}\psi_{1,\,mn})E^{+}_{mn}, & z > D \end{cases} \tag{7}$$

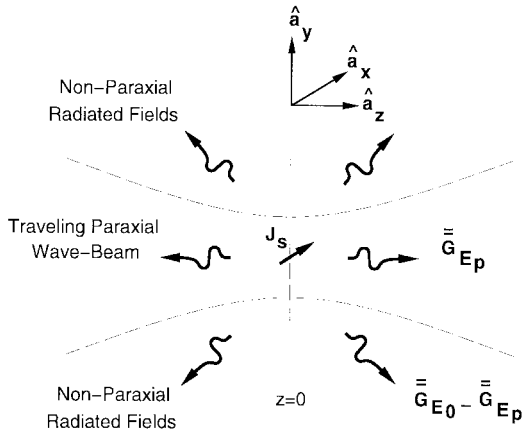

Fig. 4. Fields excited by a current element in free space.

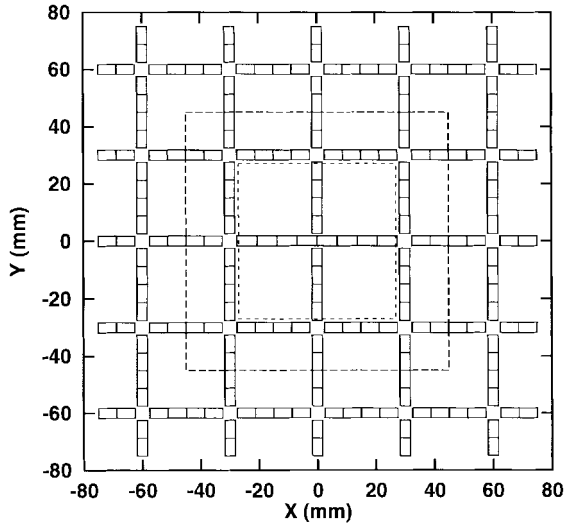

Fig. 5. A 5 × 5 QO grid along with the cell subdivision used. The dotted box indicates the extended unit cell modeled and the dashed box indicates the 3 × 3 grid modeled.

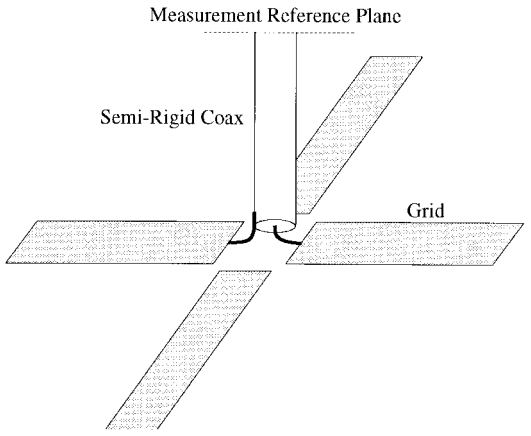

Fig. 6. Technique for measuring the driving point reflection coefficient of the finite grid array.

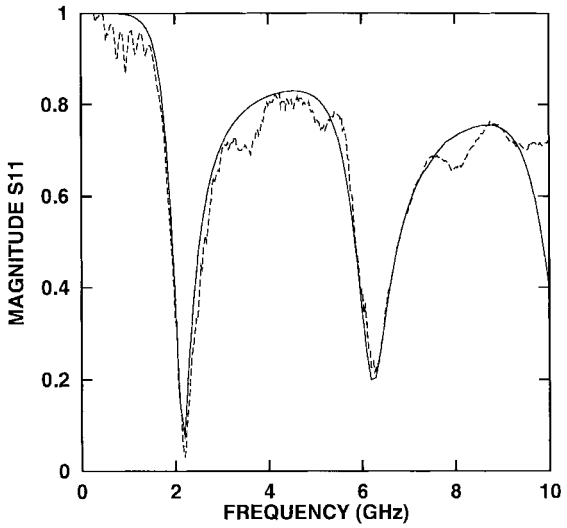

(a)

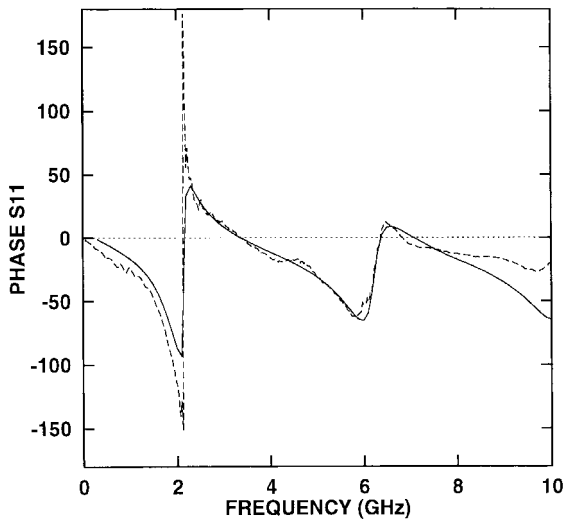

(b)

Fig. 7. Driving point reflection coefficient. (a) Magnitude and (b) phase of the unit cell: solid line, simulation; dashed line, measurement.

unit dyad, $\psi_{1,mn} = E^-_{mn}/E^+_{mn}$ and $\psi_{2,mn} = E^+_{mn}/E^-_{mn}$. Techniques for computing R_{mn} and ψ_{mn} are given in [2]. The modal Green's function contains no cross terms due to the orthogonal properties of the Hermite–Gaussian wavebeams. Also note that $\overline{\overline{\mathbf{G}}}_{Em}$ is described in the spatial domain where it is most conveniently represented.

B. Nonmodal Component—$\overline{\overline{\mathbf{G}}}_{En}$

The nonmodal component is found by removing the paraxial components $\overline{\overline{\mathbf{G}}}_{Ep}$ from the open space (i.e., free space or dielectric slab) dyadic Green's function, $\overline{\overline{\mathbf{G}}}_{E0}$ (see Fig. 4)

$$\overline{\overline{\mathbf{G}}}_{En} = \overline{\overline{\mathbf{G}}}_{E0} - \overline{\overline{\mathbf{G}}}_{Ep}. \tag{8}$$

$\overline{\overline{\mathbf{G}}}_{Ep}$ is just the paraxial (modal) component in (7) but with the lenses removed ($R_{1,mn}$, $R_{2,mn} \to 0$, and $T_{1,mn}$, $T_{2,mn} \to 1$). Spectral-domain representation of the dielectric slab

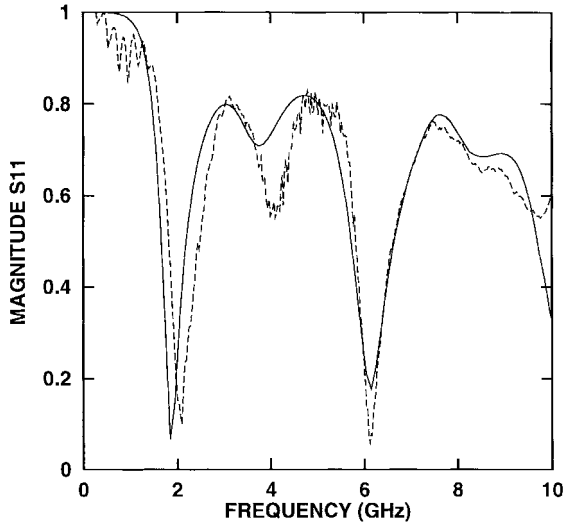

(a)

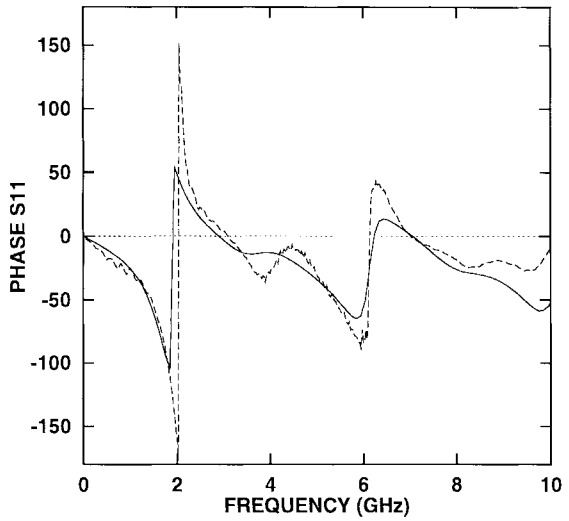

(b)

Fig. 8. Driving point reflection coefficient. (a) Magnitude and (b) phase of the 3 × 3 grid: solid line, simulation; dashed line, measurement.

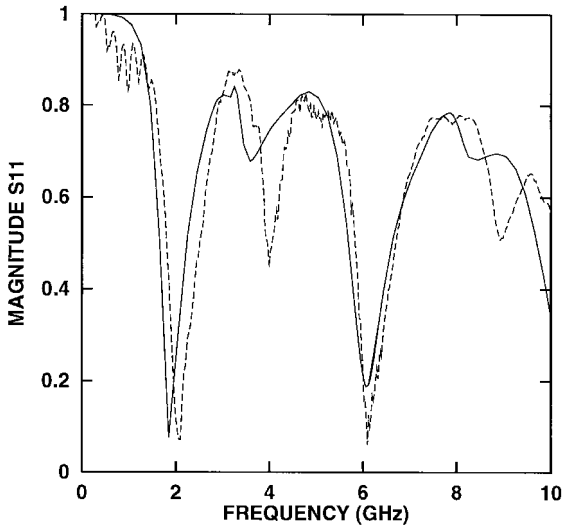

(a)

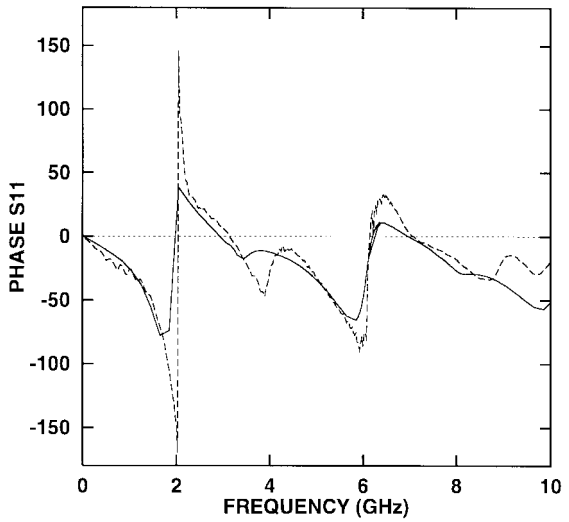

(b)

Fig. 9. Driving point reflection coefficient. (a) Magnitude and (b) phase of the 5 × 5 grid: solid line, simulation; dashed line, measurement.

Green's function $\overline{\overline{\mathbf{G}}}_{E0}$ (obtained here by using the conventional immittance approach [6]) is required to avoid the singularity that would otherwise occur when the source and observation points are co-located.

C. Final Expression

The final dyadic Green's function is evaluated in two parts, $\overline{\overline{\mathbf{G}}}_E = \overline{\overline{\mathbf{G}}}_{El} + \overline{\overline{\mathbf{G}}}_{E0}$, where $\overline{\overline{\mathbf{G}}}_{El} = \overline{\overline{\mathbf{G}}}_{Em} - \overline{\overline{\mathbf{G}}}_{Ep}$ represents the contribution of the QO modes and $\overline{\overline{\mathbf{G}}}_{E0}$ represents the free space or dielectric slab (direct radiation) contribution. (This reorganization of the Green's function from that in (2) is required to separate the spatial domain, $\overline{\overline{\mathbf{G}}}_{El}$, and spectral domain, $\overline{\overline{\mathbf{G}}}_{E0}$, formulations.) The moment-method technique developed in [4] uses a mixed spectral-domain and spatial-domain formulation and was used here to implement $\overline{\overline{\mathbf{G}}}_E$.

III. Computed and Experimental Results

Measurements and simulations were performed in the lens system of Fig. 1 for the grid structures illustrated in Fig. 5. The convex lenses were made of Rexolite 1422 ($\epsilon_r = 2.56$) with a diameter of 45.72 cm, focal length of 58.74 cm, and were spaced at twice the focal length. The grids were on a dielectric substrate with $\epsilon_r = 2.56$ and thickness 9.5 mm. The driving point reflection coefficient measurements were done using the technique shown in Fig. 6 with an HP 8510C network analyzer. The center conductor of a semirigid cable is soldered to one side of the gap and a wire conductor is soldered to the other side of the gap and outer conductor of the cable. Measurements show that this transition from the unbalanced coaxial line to the balanced twin lead line results in a small discontinuity. The calibrated reference plane is located some distance down the line from the transition (see Fig. 6) and the measurements were deembedded, taking into account the length of the line from the reference plane

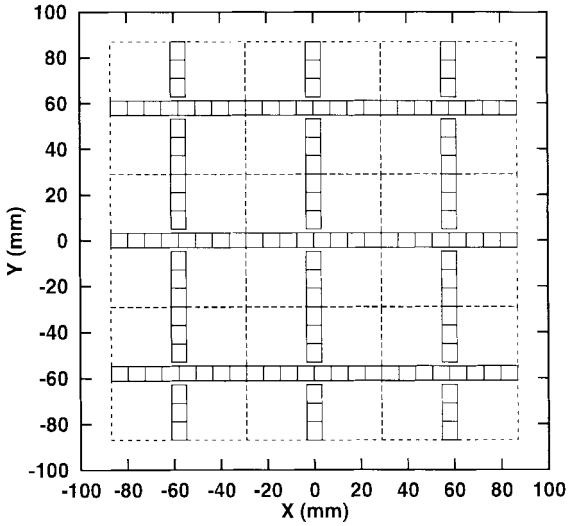

Fig. 10. A 3 × 3 QO shorted grid along with the cell subdivision used.

to the gap, and the attenuation loss of the line over this distance. The discontinuity from the transition was neglected. The cable was perpendicular to the grid with an absorber placed around the cable to avoid interference with the fields from the grid.

The driving point reflection coefficient was computed and measured at the node $x = 0$ and $y = 0$ with all the other gaps left opened and is shown in Figs. 7–9 for the extended unit cell, 3×3 grid, and 5×5 grid. The extended unit cell was used instead of a standard unit cell to match resonant frequencies with the 3×3 and 5×5 grids. The unit cell or extended unit cell has no meaning on its own and is only used here for comparison with the other grid arrays. From these results, one can observe that there is mutual coupling between the grid elements, which is nonexistent in the extended unit cell. The difference between the 3×3 and 5×5 grids is small, but more mutual coupling is noticed in the latter. The simulations were efficient requiring 50 s per frequency point and 5 Mbytes for simulations of the 5×5 grid.

To illustrate edge effects of finite grids, simulations and measurements for the grid shown in Fig. 10 were performed for the center and corner gaps with all the other gaps in the grid shorted. The results are shown in Fig. 11 for both cases. The measurements are less accurate for the edge and corner gaps due to the symmetry lost in the structure since a balun is not used. The results indicate that the input impedance of edge and corner gaps differ from that of the middle gap due to the finite extent of the grid. This variation, as well as the direct coupling between cells, is not incorporated in unit-cell-based modeling of QO systems [8]. The unit-cell approach assumes the grid array to be infinitely periodic. With this assumption, the grid structure is modeled by only considering the unit cell with magnetic- and electric-wall boundary conditions applied to the outer edges of the unit cell to emulate an infinite grid array. Therefore, the coupling that is considered is a result of these boundary conditions and does not account for direct coupling from nearby unit cells. Due to the differences in the unit-cell formulation and the finite grid formulation, it is difficult to show a direct comparison between the two methods.

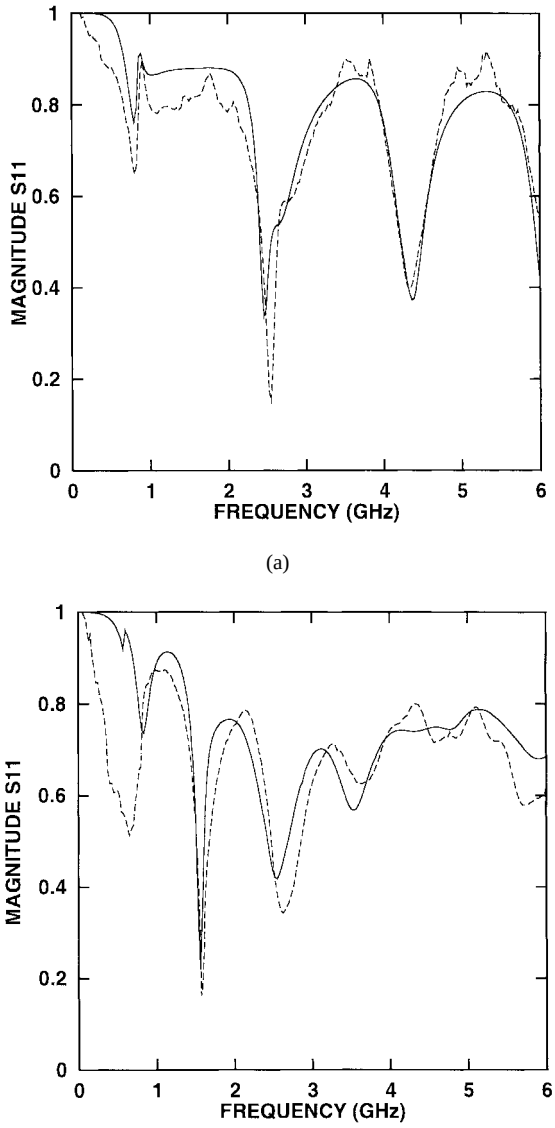

(a)

(b)

Fig. 11. Driving point reflection coefficient magnitude. (a) Middle gap and (b) corner gap of the 3 × 3 shorted grid: solid line, simulation; dashed line, measurement.

IV. Conclusion

A full-wave moment-method implementation has been developed for the analysis of finite grid structures in a QO lens system. This implementation includes the derivation of a dyadic Green's function for this system and a moment-method scheme utilizing both spatial and spectral domains for efficient and numerically stable computation of the moment matrix elements. As a verification of the moment method, simulated results have been shown to compare favorably with measurements. The significance of the modeling work is that: 1) finite sized grids are considered and 2) it is broadband (from dc to any frequency) as required in CAE. From a

system development point of view, the design of each element in the array can be individually optimized to achieve an optimum global solution in terms of stability, output power, and efficiency.

The moment-method simulator is currently being used to find the multiport parameters from a finite grid array. In this analysis, each unit cell in the grid array is characterized as a four-port network with the ports defined to be at the terminals of the gap with respect to a common reference terminal. The 5×5 grid array presented in this paper is represented as a 100-port network with coupling considered between all ports. The port matrix, computed with the moment-method simulator, is converted to a nodal admittance matrix, which is then incorporated into a microwave circuit simulator such as harmonic balance.

REFERENCES

[1] J. W. Mink, "Quasi-optical power combining of solid-state millimeter-wave sources," *IEEE Trans. Microwave Theory Tech.*, vol. MTT-34, pp. 273–279, Feb. 1986.

[2] P. L. Heron, G. P. Monahan, J. W. Mink, F. K. Schwering, and M. B. Steer, "Impedance matrix of an antenna array in a quasi-optical resonator," *IEEE Trans. Microwave Theory Tech.*, vol. 41, pp. 1816–1826, Oct. 1993.

[3] P. L. Heron, F. K. Schwering, G. P. Monahan, J. W. Mink, and M. B. Steer, "A dyadic Green's function for the plano-concave quasi-optical resonator," *IEEE Microwave Guided Wave Lett.*, vol. 3, pp. 256–258, Aug. 1993.

[4] T. W. Nuteson, G. P. Monahan, M. B. Steer, K. Naishadham, J. W. Mink, K. K. Kojucharow, and J. Harvey, "Full-wave analysis of quasi-optical structures," *IEEE Trans. Microwave Theory Tech.*, vol. 44, pp. 701–710, May 1996.

[5] T. W. Nuteson, M. B. Steer, K. Naishadham, J. W. Mink, and J. Harvey, "Electromagnetic modeling of finite grid structures in quasi-optical systems," in *IEEE MTT-S Int. Microwave Symp. Dig.*, San Francisco, CA, June 1996, pp. 1251–1254.

[6] T. Itoh, "Spectral domain immittance approach for dispersion characteristics of generalized printed transmission lines," *IEEE Trans. Microwave Theory Tech.*, vol. MTT-28, pp. 733–736, July 1980.

[7] D. M. Pozar, "Input impedance and mutual coupling of rectangular microstrip antennas," *IEEE Trans. Antennas Propagat.*, vol. AP-30, pp. 1191–1196, Nov. 1982.

[8] S. C. Bundy and Z. B. Popović, "A generalized analysis for grid oscillator design," *IEEE Trans. Microwave Theory Tech.*, vol. 42, pp. 2486–2491, Dec. 1994.

Todd W. Nuteson (S'90–M'97) was born in Tacoma, WA, on November 16, 1967. He received the B.S. and M.S. degrees, both in electrical engineering, from Wright State University, Dayton, OH, in 1991 and 1993, respectively, and the Ph.D. degree in electrical engineering from North Carolina State University, Raleigh, in 1996.

He is currently working as a Post-Doctoral Fellow with the Electronics Research Laboratory, North Carolina State University, doing research in spatial power combining systems. From 1991 to 1993, he worked at Wright State University as a Research and Teaching Assistant where he received AFOSR graduate research fellowships in 1992 and 1993. From 1993 to 1996, he worked at North Carolina State University as a Research Assistant with the Electronics Research Laboratory, Department of Electrical and Computer Engineering, performing research in moment-method solutions for quasi-optics (QO) systems. His research interests include numerical modeling of microwave and millimeter-wave circuits, QO, and spatial power combining, antennas, and electromagnetics.

Dr. Nuteson won the Prestigious Bronze Medallion for Outstanding Scientific Achievement presented at the 20th Army Science Conference.

Huan-Sheng Hwang (S'93) received the B.S.E.E. degree from Tutung Institute of Technology, Taipei, Taiwan, in 1984, and the M.S.E.E. degree from North Carolina State University, Raleigh, in 1993. Currently, he is working toward the Ph.D. degree while working at the Electronics Research Laboratory, North Carolina State University, doing research in quasi-optics (QO) power combining systems.

He is the coauthor of a book chapter, "Dielectric Slab Combiners," in *Active and Quasi-Optical Arrays*. His research interests include QO and spatial power combining system, antennas, electromagnetics, microwave and millimeter-wave circuits, and optics.

Mr. Hwang won the Prestigious Bronze Medallion for Outstanding Scientific Achievement presented at the 20th Army Science Conference in 1996.

Michael B. Steer (S'76–M'78–SM'90) received the B.E. and Ph.D. degrees in electrical engineering from the University of Queensland, Brisbane, Australia, in 1978 and 1983, respectively.

He is currently Director of the Electronics Research Laboratory and Professor of electrical and computer engineering at North Carolina State University, Raleigh. His expertise in teaching and research involves circuit design methodology and taught courses in circuit design, including basic circuit design, analog integrated-circuit design, RF and microwave circuit design, solid-state devices, and computer-aided circuit analysis. He teaches video-based courses on computer-aided circuit analysis and on RF design for wireless, which are broadcast nationally by the National Technological University. His research has been directed at developing RF and microwave design methodologies. Throughout his career this work has been closely tied to the development of microwave circuits and solving fundamental problems in both high-speed digital and microwave-circuit implementations. He has authored or co-authored over 110 papers on topics related to RF and microwave design methodology. Currently his interests are in the CAE of quasi-optics (QO) power combining systems, the implementation of a two-dimensional QO power combining system, high-efficiency, low-cost RF technologies for wireless applications, and computer-aided engineering of mixed digital, analog, and microwave circuits.

Dr. Steer is active in the IEEE Microwave Theory and Techniques (MTT) Society, where he serves on the technical committees on field theory and on CAD, and is secretary of the Society for 1997. He is a member of the International Union of Radio Science (URSI), Commission D. He is a 1987 Presidential Young Investigator. He has worked on projects sponsored by the National Science Foundation, the U.S. Army Research Office, SEMATECH, Airforce Office of Scientific Research, Defense Advanced Research Projects Agency, BNR, DEC, IBM, Analog Devices, Compact Software, and Scientific Research Associates.

Krishna Naishadham (S'84–M'86) received the M.S. degree from Syracuse University, Syracuse, NY, and the Ph.D. degree, both in electrical engineering, from the University of Mississippi, Jackson, in 1982 and 1987, respectively.

From 1987 to 1990, he was an Assistant Professor in electrical engineering at the University of Kentucky, Lexington. In August 1990, he joined the Department of Electrical Engineering, Wright State University, Dayton, OH, where he is currently an Associate Professor. His research interests are in the areas of computational electromagnetics, design and analysis of microwave and millimeter-wave integrated circuits (MMIC's), prediction of EMI in printed circuit boards, and electronic materials.

Dr. Naishadham is a member of Eta Kappa Nu and Phi Kappa Phi and an elected member of URSI Commission B. He serves on the Analytic and Numerical Methods Committee (Comm. P) of the IEEE Microwave Theory and Techniques Society. He received the Best Session Paper award at the 7th SAMPE Conference on Electronic Materials.

James F. Harvey (M'91) received the B.S. degree in engineering from the U.S. Military Academy, West Point, NY, in 1964, the M.A. degree in physics from Dartmouth College, Hanover, NH, in 1972, and his Ph.D. degree in applied science from the University of California, Davis, in 1991, with research performed at Lawrence Livermore National Laboratory.

He is currently a Program Manager at the U.S. Army Research Office, Triangle Park, NC, with primary responsibility within the fields of electromagnetics, millimeter-wave circuit integration, low-power/minimum-power system design, and the electronic aspects of demining. His personal research interests are in the fields of quasi-optics and millimeter-wave devices.

Dr. Harvey is active in the IEEE MTT Society, the IEEE Lasers and Electro-Optics Society, URSI, and the American Physical Society.

James W. Mink (S'59–M'65–SM'81–F'91) received the Ph.D. degree in electrical engineering from the University of Wisconsin–Madison, in 1964.

In 1994, he joined North Carolina State University, Raleigh, on a full-time basis where he is now a Visiting Professor and Graduate Coordinator in the Department of Electrical and Computer Engineering. His research continues to focus upon conformal antennas, in particular as applied to wireless communications and upon millimeter-wave systems and devices. From 1976 to 1994, he was employed by the U.S. Army Research Office, cumulating his service as the Director of the Electronics Division. He has published or presented approximately 60 refereed papers, holds 6 patents, and was associate editor of the IEEE Press's *Channel Characterization*.

Dr. Mink is a member of the IEEE Antennas and Propagation Society Best Paper Awards Committee from 1982 to the present. He also has served on the Centennial Medals Committee. In addition, from 1979 through 1994, he served as the principal Army representative of the Joint Services Electronics Program. Since 1987, he has served as a program evaluator for ABET, continuing to serve in that capacity. He served as guest editor for two IEEE-MTT special issues entitled "Quasi-Optical Techniques" and "Numerical Methods." He was an associate editor for IEEE TRANSACTIONS ON ANTENNAS AND PROPAGATION from 1983 to 1989, and is currently a member of APS ADCOM. He was awarded the Superior Civilian Service Award for his program management achievements, two Bronze medals, and two Research and Development Awards for technical achievements by the Department of the U.S. Army.